Buckling and Postbuckling Behavior of Composite Cylindrical Shells under Axial Compression

N. S. KHOT*
Air Force Flight Dynamics Laboratory, Wright-Patterson Air Force Base, Ohio

A theoretical analysis of the buckling and postbuckling equilibrium behavior of a fiber reinforced cylindrical shell under uniform axial compression is presented. The investigation also includes some data on the effect of initial imperfections on the buckling behavior of fiber reinforced cylindrical shells. von Kármán-Donnell large displacement equations and the principle of stationary potential energy are applied to study the postbuckling behavior. The results are given for various fiber orientations in the three-layer shell having a radius-to-thickness ratio of 166.77, consisting of either glass-epoxy or boron-epoxy composites. The cases when the stiffness coupling matrix is not equal to zero and the coupling matrix is set equal to zero are considered. It is shown that the latter simplifying assumption gives unconservative buckling and postbuckling loads. From the results of the effect of initial imperfections on the buckling behavior, it is seen that the boron-epoxy composite shells are less imperfection sensitive than glass-epoxy composite shells. This investigation shows that, in general, composite shells are less imperfection sensitive than isotropic shells.

Nomenclature

A,D,D^*,d^* = stiffness matrices of material
a,d = compliance matrices of material
E_{11},E_{22},E_{12} = elastic constants
F = stress function
F_i,G_i,H_i = quantities defined in Appendices A and C
h_k = z coordinate of common boundary between kth and $(k\text{-}1)$th layers
k_x,k_y,k_{xy} = changes in curvatures of reference surface
L = length of cylinder
l_x,l_y = axial and circumferential half wavelengths of radial displacement
$\bar{l}_x,\bar{l}_y$ = axial and circumferential half wavelengths of initial imperfection
M_x,M_y,M_{xy} = moment results
N_x,N_y,N_{xy} = stress resultants
n = number of laminas in shell thickness
N = number of circumferential waves
P_1,P_2,P_3,P_4 = modified radial deflection parameters
R = radius of shell
R_i,T_i = quantities defined in Appendices B and C
U,V,W = axial, circumferential, and radial displacements of reference surface
$\bar{W}^*$ = imperfection parameter $\left(\sum_{i-1}^{4} \bar{W}_i \Big/ \text{thickness of shell}\right)$
$\bar{W}$ = initial imperfection of reference surface in radial direction
W_0,W_1,W_2,W_3,W_4 = radial deflection parameters
$\bar{W}_1,\bar{W}_2,\bar{W}_3,\bar{W}_4$ = amplitudes of initial perfection $\bar{W}$
x,y,z = axial, circumferential, radial coordinates of reference surface
$\alpha,\beta,\gamma,\nu,\xi,\kappa,\lambda,\psi,\rho,\phi$ = stiffness parameter as defined in Eq. (24)
θ = fiber orientation
$\bar{\varepsilon}$ = end shortening (in./in.), $\varepsilon = (\bar{\varepsilon}R/2)(a_{11}d_{22}^*)^{-1/2}$
$\bar{\sigma}$ = average axial compressive unit load
σ = $(\bar{\sigma}R/2)(a_{11}/d_{22}^*)^{1/2}$
$\bar{\sigma}_{cl}$ = classical buckling load (lb/in.)
σ_{cl} = $(\bar{\sigma}_{cl}R/2)(a_{11}/d_{22}^*)^{1/2}$
$\bar{\sigma}_{max}$ = maximum load an imperfect shell can support befor snap-through
$\bar{\mu}$ = l_y/l_x, wavelength ratio
μ = $\bar{\mu}(a_{22}/a_{11})^{1/4}$
ω = $R(a_{22}d_{22}^*)^{-1/2}/N^2$

Received October 28, 1968; presented at the AIAA/ASME 10th Structures, Structural Dynamics and Materials Conference, New Orleans, La., April 14–16, 1969 (no paper number; published in bound volume of conference papers); revision received August 6, 1969.

* Aerospace Engineer, Structures Division. Member AIAA.

1. Introduction

THIS investigation deals with the buckling and postbuckling equilibrium behavior of multilayer anisotropic cylindrical shells subjected to uniform axial compressive end loads. Some results are also presented on the influence of initial imperfections on the maximum load the shell can support prior to buckling. The study was prompted by the increasing use of fiber reinforced structures in aerospace industry.

The buckling of filament-wound cylinders under axial compression has been analytically and experimentally investigated by Tasi, Feldman, and Stang.[1] The experimental loads were found to lie within 65% to 85% of theoretically predicted loads. Tasi[2] has investigated the effect of heterogeneity on the stability of composite cylindrical shells. He considered shells where the in-plane, coupling, and bending stiffness matrices are orthotropic. His results show that heterogeneity has a deleterious effect on the stability of composite cylinders.

In the present investigation, the postbuckling equilibrium behavior is studied through the application of the principle of stationary potential energy. This nonlinear analysis, where von Kármán-Donnell large-displacement equations are used is analogous to the commonly applied energy analysis to isotropic and orthotropic cylindrical shells.[3–10] In this study, the total potential energy is not considered as a continuous function of a circumferential wavelength parameter.[7] The postbuckling equilibrium states are then represented by a family of load-shortening curves; each curve gives a relative minimum postbuckling load corresponding to the specified wave number. From the practical point of view, the minimum postbuckling load may not have quantitative significance but it generally indicates the imperfection sensitivity of the structure. An excellent comprehensive survey on the results of postbuckling investigations of cylindrical shells during the last 30 years may be found in Ref. 11.

The numerical results presented in this paper are for a three-layer glass-epoxy and boron-epoxy composite cylindrical

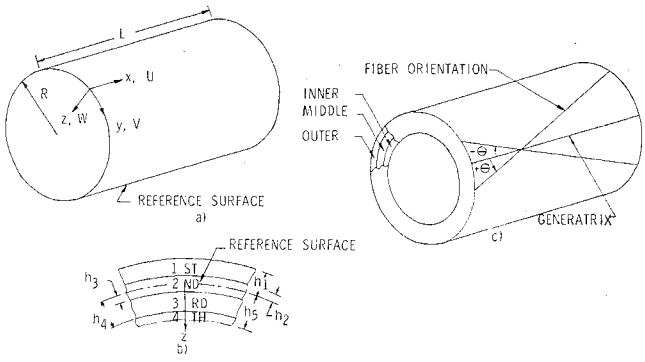

Fig. 1 Geometry.

shell with a radius-to-thickness ratio of 166.67. It is observed that neglecting the stiffness coupling matrix gives unconservative buckling loads as well as postbuckling loads. The circumferential wave number corresponding to the smallest value of the relative minimum postbuckling load is found to depend primarily on the radius-to-thickness ratio and is independent of material and fiber orientation. The composite shells appear to be less imperfection sensitive than isotropic shells. Glass-epoxy is more imperfection sensitive than boron-epoxy.

2. Analytical Formulation

In deriving the equations, the coordinate system (x,y,z) shown in Fig. 1a has been used.

2.1 Strain-Displacement Relations

The axial, circumferential, and shear strains at a point within the shell thickness corresponding to Love-Kirchhoff assumptions are

$$\mathcal{E}_x = \epsilon_x - zk_x,\ \mathcal{E}_y = \epsilon_y - zk_y,\ \mathcal{E}_{xy} = \epsilon_{xy} - zk_{xy} \tag{1}$$

where ϵ_x, ϵ_y, ϵ_{xy} are the strains on the reference surface and k_x, k_y, k_{xy} are the changes in curvature.

For a cylindrical shell of radius R, the von Kármán-Donnell nonlinear strain-displacement relations and the changes of curvatures on the reference surface may be written as

$$\begin{aligned} \epsilon_x &= U_{,x} + \tfrac{1}{2}(W_{,x})^2 \\ \epsilon_y &= V_{,y} + \tfrac{1}{2}(W_{,y})^2 - (W/R) \\ \epsilon_{xy} &= U_{,y} + V_{,x} + W_{,x}W_{,y} \end{aligned} \tag{2}$$

$$k_x = W_{,xx}\ k_y = W_{,yy}\ k_{xy} = 2W_{,xy} \tag{3}$$

Where $U(x,y)$, $V(x,y)$, and $W(x,y)$ are the axial, circumferential, and radial displacements of the reference surface. A comma placed after the function denotes differentiation with respect to the coordinate.

2.2 Constitutive Equations

The constitutive relations for the composite shell are[12]

$$[\epsilon] = [a][N] + [d]^T[k] \tag{4}$$

$$[M] = [d][N] - [d^*][k] \tag{5}$$

The elements of the matrices $[a]$, $[d]$, and $[d^*]$ are defined by

$$[a] = [A]^{-1};\ [d] = [D][a] \tag{6}$$

$$[d^*] = [D^*] - [D][a][D] \tag{7}$$

with in-plane, coupling, and bending stiffness matrices $[A]$, $[D]$, $[D^*]$ defined in terms of the individual layer elastic moduli $[C^{(k)}]$ by

$$\begin{aligned} A_{ij} &= \sum_{k=1}^{n} C_{ij}^{(k)}(h_{k+1} - h_k) \\ D_{ij} &= \frac{1}{2}\sum_{k=1}^{n} C_{ij}^{(k)}(h_{k+1}^2 - h_k^2) \\ D_{ij}^* &= \frac{1}{3}\sum_{k=1}^{n} (h_{k+1}^3 - h_k^3) \end{aligned} \tag{8}$$

where the index k denotes the kth layer bounded by z coordinates h_k and h_{k+1} (see Fig. 1b).

2.3 Potential Energy

The total potential energy of a multilayered cylindrical shell of radius R and length L can be written as

$$\Pi = V_1 + V_2 + V_3 \tag{9}$$

where

$$\begin{aligned} V_1 &= \frac{1}{2}\int_0^L\int_0^{2\pi R} [N]^T[a][N]dxdy \\ V_2 &= \frac{1}{2}\int_0^L\int_0^{2\pi R} [k]^T[d^*][k]dxdy \end{aligned} \tag{10}$$

and the potential energy of the applied axial end load

$$V_3 = -\int_0^{2\pi R} [N_x]_{x=L}\,dy \int_0^L U_{,x}dx \tag{11}$$

2.4 Equilibrium and Compatibility Equations

The first variation of the total potential energy with respect to U, V, W equated to zero yields the natural boundary conditions and the following set of equilibrium equations:

$$N_{x,x} + N_{xy,y} = 0,\ N_{y,y} + N_{xy,x} = 0 \tag{12}$$

$$(N_y/R) + N_xW_{,xx} + 2N_{xy}W_{,xy} + N_yW_{,yy} + M_{x,xx} + 2M_{xy,xy} + M_{y,yy} = 0 \tag{13}$$

Equation (12) is identically satisfied by the introduction of an Airy stress function $F(x,y)$ defined as follows:

$$N_x = F_{,yy},\ N_y = F_{,xx},\ N_{xy} = -F_{,xy} \tag{14}$$

The equilibrium equation (13) with the aid of Eqs. (6, 7, and 14) can be expressed as

$$\begin{aligned} &d_{12}F_{,xxxx} + (2d_{62} - d_{16})F_{,xxxy} + (d_{11} + d_{22} - 2d_{66})F_{,xxyy} + \\ &(2d_{61} - d_{26})F_{,xyyy} + d_{21}F_{,yyyy} + N_y(W_{,yy} + 1/R) + \\ &N_xW_{,xx} + 2N_{xy}W_{,xy} - d_{11}^*W_{,xxxx} - 4d_{16}^*W_{,xxxy} - \\ &(2d_{12}^* + 4d_{66}^*)W_{,xxyy} - 4d_{26}^*W_{,xyyy} - \\ &d_{22}^*W_{,yyyy} = 0 \end{aligned} \tag{15}$$

Eliminating U and V from Eq. (2) and utilizing Eqs. (4) and (5) the following compatibility condition is obtained:

$$\begin{aligned} &a_{22}F_{,xxxx} - 2a_{26}F_{,xxxy} + (2a_{12} + a_{66})F_{,xxyy} - 2a_{16}F_{,xyyy} + \\ &a_{11}F_{,yyyy} = -d_{12}W_{,xxxx} - (2d_{61} - d_{26})W_{,xyyy} - d_{21}W_{,yyyy} + \\ &(W_{,xy})^2 - W_{,xx}W_{,yy} - W_{,xx}(1/R) - (2d_{62} - d_{16})W_{,xxxy} - \\ &(d_{11} + d_{22} - 2d_{66})W_{,xxyy} \end{aligned} \tag{16}$$

2.5 Assumed Radial Deflection Function and Compatible Stress Function

The approximate radial deflection function W is taken in the following form:

$$W = W_0 + W_1\cos\frac{\pi x}{l_x}\cos\frac{\pi y}{l_y} + W_2\cos\frac{2\pi x}{l_x} + W_3\cos\frac{2\pi x}{l_x}\cos\frac{2\pi y}{l_y} + W_4\cos\frac{4\pi x}{l_x} \tag{17}$$

where W_0 through W_4 are undetermined displacement parameters, and l_x and l_y are the half-wavelengths in the axial and circumferential directions. This form is identical to that used by Almroth (Ref. 5, case B) for the postbuckling analysis of an isotropic cylindrical shell. Equation (17) corresponds to a shell whose ends are neither clamped nor simply supported; however, as has been pointed out in the past, the boundary conditions may not influence the postbuckling behavior if the shell length is sufficient. It is also assumed that the shell may not deform into a torsional buckling mode.

In order to determine the stress function F, the expression for W [Eq. (17)] is substituted into the compatibility equation [Eq. (16)] and solved for F. After imposing the condition that the axial membrane stresses are in over-all equilibrium with the applied compressive load $\bar{\sigma}$, the solution of Eq. (16) can be written as

$$F = \bar{F} - \bar{\sigma}y^2/2 \tag{18}$$

The expression for $\bar{F}$ is given in Appendix A.

2.6 Unit End Shortening and Uniform Radial Displacement

The unit end shortening $\bar{\varepsilon}$ caused by the applied compressive end load is given by

$$\bar{\varepsilon} = -\frac{1}{L}\int_0^L U_{,x}dx \tag{19}$$

Utilizing Eqs. (2, 4, 5, 17, and 18) end shortening can be expressed as

$$\bar{\varepsilon} = a_{11}\bar{\sigma} + (W_1^2 + 8W_2^2 + 4W_3^2 + 32W_4^2)\pi^2/8l_x^2 \tag{20}$$

Imposing the condition that the circumferential displacement V be single valued, i.e.,

$$\int_0^{2\pi R} V_{,y}dy = 0$$

and using Eqs. (2, 4, 5, 17, and 18) would yield

$$W_0 = Ra_{12}\bar{\sigma} + (W_1^2 + 4W_3^2)\pi^2R/8l_y^2 \tag{21}$$

2.7 Total Potential Energy

Upon substitution of the expressions for W and F into Eq. (9) and integration, the total potential energy can be written in the following form:

$$\begin{aligned}
\mathrm{II}\,\frac{4R}{\pi L d_{22}^*} = \frac{1}{\omega^2}\Bigg(&\frac{1}{T_1^2 - T_2^2}[T_1\{T_3^2P_1^2 + T_4^2(P_1^2 + 16P_3^2) + 16T_{13}^2P_3^2 + 4T_3P_1^2P_2\mu^2 + 64T_{13}P_3^2P_4\mu^2 + 64P_3^2P_4^2\mu^4 + 4P_1^2P_2^2\mu^4\} + T_2T_4\{2T_3P_1^2 + 32T_{13}P_3^2 + 4P_1^2P_2\mu^2 + 64P_3^2P_4\mu^2\}] + \frac{1}{T_5^2 - T_6^2}[T_5\{4P_1P_3 + 2P_1P_2 + 8P_1P_4\}^2\mu^4 + 64P_3^2P_4^2\mu^4] + \\
&\frac{1}{T_7^2 - T_8^2}[16T_7P_1^2P_3^2\mu^4] + \frac{1}{T_9^2 - T_{10}^2}[64T_9P_1^2P_4^2\mu^4] + \\
&\frac{1}{T_{11}^2 - T_{12}^2} \times [4T_{11}P_2^2P_3^2\mu^4] + \Big[2P_2^2\omega^2 + 2P_4^2\omega^2 + \frac{1}{32}P_1^4 + \frac{1}{2}P_3^4 - \frac{1}{2}P_1^2P_2\omega - 2P_3^2P_4\omega + P_1^2 + 16P_3^2\Big] + \Big[32\kappa^2P_2^2 + 512\kappa^2P_4^2 + \frac{P_1^4}{32} + \frac{P_3^4}{2} + 8P_2^2P_3^2 + P_1^2P_2P_3 + P_1^2\phi + 32P_2^2\phi + 16P_3^2\phi + 512P_4^2\phi\Big]\mu^4 + \\
&\kappa[P_1^2P_2 + 16P_3^2P_4]2\mu^2 - \kappa[P_2^2 + 4P_4^2]16\mu^2\omega + \rho\phi^{1/2}[P_1^2 + 16P_3^2]2\mu^2 - [P_1^2 + 8P_2^2 + 4P_3^2 + 32P_4^2]2\mu^2\omega\sigma\Bigg) + \text{constants}
\end{aligned} \tag{22}$$

where

$$\begin{aligned}
&P_i = W_i(a_{22}d_{22}^*)^{-1/2},\ i = 1\text{–}4 \\
&\mu = \frac{l_y}{l_x}\left(\frac{a_{22}}{a_{11}}\right)^{1/4},\ \omega = \frac{R(a_{22}d_{22}^*)^{-1/2}}{N^2} \\
&\sigma = (\bar{\sigma}R/2)(a_{11}/d_{22}^*)^{1/2},\ N = \pi R/l_y
\end{aligned} \tag{23}$$

and the functions T_1 through T_{13} are listed in Appendix B. The stiffness parameters which appear in the energy expression and in the functions T_1 through T_{13} are defined below:

$$\begin{aligned}
&\alpha = (2a_{12} + a_{66})(a_{11}a_{22})^{-1/2},\ \beta = a_{26}a_{11}^{-1/4}a_{22}^{-3/4} \\
&\gamma = a_{16}a_{22}^{-1/4}a_{11}^{-3/4},\ \nu = (2d_{62} - d_{16})(a_{22}d_{22}^*)^{-1/2}\left(\frac{a_{11}}{a_{22}}\right)^{1/4} \\
&\xi = (2d_{61} - d_{26})(a_{22}d_{22}^*)^{-1/2}\left(\frac{a_{22}}{a_{11}}\right)^{1/4} \\
&\kappa = \frac{d_{12}}{a_{22}}\left(\frac{a_{11}}{d_{22}^*}\right)^{1/2},\ \lambda = d_{21}(a_{11}d_{22}^*)^{-1/2} \\
&\psi = (d_{11} + d_{22} - 2d_{66})(a_{22}d_{22}^*)^{-1/2} \\
&\rho = (d_{12}^* + 2d_{66}^*)(d_{11}^*d_{22}^*)^{-1/2},\ \phi = (a_{11}d_{11}^*)/(a_{22}d_{22}^*)
\end{aligned} \tag{24}$$

The 21 elements in matrices $[a]$, $[d]$, and $[d^*]$ are reduced to the 10 stiffness parameters defined previously. The elements d_{16}^* and d_{26}^* are absent in Eq. (24). The integrals associated with these elements in Eq. (10) vanish for the assumed radial deflection function. When the coupling matrix $[D]$ is zero, the stiffness parameters ν, ξ, κ, λ, and ψ vanish. For the special case of orthotropic material where the reference axes coincide with the elastic axes, all parameters except α, ρ, and ϕ are zero. When the material is isotropic $\alpha/2 = \rho = \phi = 1$.

The end shortening $\bar{\varepsilon}$ [Eq. (20)] may be redefined as a new parameter ε,

$$\varepsilon = \sigma + \tfrac{1}{16}(P_1^2 + 8P_2^2 + 4P_3^2 + 32P_4^2)\mu^2/\omega \tag{25}$$

where

$$\varepsilon = \bar{\varepsilon}R/2(a_{11}d_{22}^*)^{1/2}$$

For a system in equilibrium, with given values of stiffness parameters, circumferential wave number parameter, ω, and load parameter, σ, the principle of stationary potential energy requires that the function II [Eq. (22)] attain a stationary value for small variations of P_1, P_2, P_3, P_4, and μ. Here variation of the total potential energy with respect to μ may be permissible since the cylinder is not assumed to be of fixed length. Application of the preceding principle is equivalent to

$$\frac{\partial \mathrm{II}}{\partial P_1} = \frac{\partial \mathrm{II}}{\partial P_2} = \frac{\partial \mathrm{II}}{\partial P_3} = \frac{\partial \mathrm{II}}{\partial P_4} = \frac{\partial \mathrm{II}}{\partial \mu} = 0 \tag{26}$$

For want of space, the lengthy nonlinear algebraic equations generated by Eq. (26) are not given here.

2.8 Numerical Analysis

To investigate the postbuckling behavior and to determine the unknown parameters, Eq. (26) must be solved. In the numerical work this was accomplished by the use of Newton-Raphson iterative method. Knowing the unknown parameters, Eqs. (23) and (25) can be used to evaluate $\bar{\varepsilon}$, $\bar{\sigma}$ and plot $\bar{\varepsilon}$ vs $\bar{\sigma}$ curves for different values of N.

2.9 Classical Buckling Load

The total potential energy based on the linear theory can be obtained from Eq. (22) by retaining terms of second order in P_1 only. Then minimizing this expression with respect to P_1

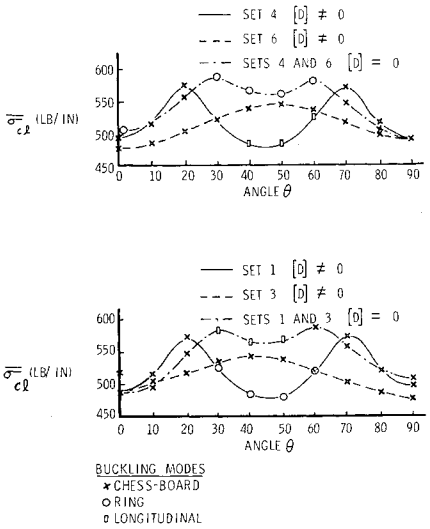

Fig. 2 Classical buckling loads for glass-epoxy composite shells.

the following expression is obtained:

$$\sigma_{cl} = R_1[R_2/\omega + R_3\omega + R_4] + R_5/\omega \tag{27}$$

where the functions R_1 through R_5 are as given in Appendix C. The conditions for the critical value of the classical buckling load are obtained by minimizing Eq. (27) with respect to $a(=\mu^2)$ and ω. These two conditions are

$$R_{11}/\omega + \omega R_{12} + R_{13} = 0 \tag{28}$$

and

$$\omega = [(R_1R_2 + R_5)/R_1R_3]^{1/2} \tag{29}$$

where the functions R_1 through R_{13} are as given in Appendix C. Eliminating ω between Eqs. (28) and (29) yields

$$R_{11}\left(\frac{R_1R_3}{R_1R_2 + R_5}\right)^{1/2} + R_{12}\left(\frac{R_1R_2 + R_5}{R_1R_3}\right)^{1/2} + R_{13} = 0 \tag{30}$$

Solution of Eq. (30) gives the value of a for which σ_{cl} in Eq. (27) is minimum. From the physical point of view only a real positive value of a is acceptable. The solution to Eq. (30) can be obtained by the Newton-Raphson iterative method. The possible solutions of Eq. (30) are $0 < a < \infty$ (chess-board buckling); $a = \infty$ (ring buckling) and $a = 0$ (longitudinal buckling). In the latter two cases the critical value of σ_{cl} can

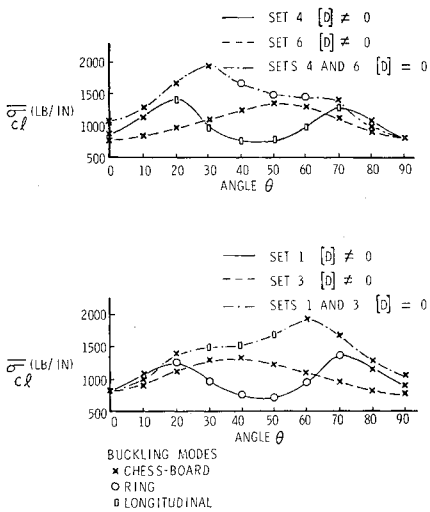

Fig. 3 Classical buckling loads for boron-epoxy composite shells.

Table 1 Elastic properties of materials

Glass-epoxy	Boron-epoxy
$E_{11} = 7.5 \times 10^6$ psi	$E_{11} = 40.0 \times 10^6$
$E_{22} = 3.5 \times 10^6$ psi	$E_{22} = 4.5 \times 10^6$
$\nu_{12} = 0.25$	$\nu_{12} = 0.25$
$G = 1.25 \times 10^6$ psi	$G = 1.5 \times 10^6$
$\nu_{21} = \nu_{12}E_{22}/E_{11}$	

be obtained by letting a approach infinity and zero, respectively. Thus

$$\sigma_{cl}(\text{ring}) = (\kappa^2 + \phi)^{1/2} - \kappa$$
$$\sigma_{cl}(\text{long}) = (\lambda^2 + 1)^{1/2} - \lambda \tag{31}$$

From the three types of buckling modes, that mode may appear which is connected with the smallest value of σ_{cl}. For an orthotropic shell where all parameters are zero except α, ρ, and ϕ, the Eqs. (27–31) reduce to those given in Ref. 6. For an isotropic shell where $\alpha/2 = \rho = \phi = 1$ and all other stiffness parameters are zero, $\sigma_{cl} = 1$ for all the buckling modes.

3. Numerical Analysis of a Three-Layer Shell

Since the possible stiffness parameter variations are so numerous, only the behavior of a shell of fixed geometry, but with different material and fiber orientations is investigated. A three-layer shell with a radius of 6.0 in. and the thickness of each layer equal to 0.012 in. is selected for this purpose. The midsurface is the reference surface. All layers consist of either glass-epoxy or boron-epoxy composites with fibers oriented in different directions in each layer. The elastic properties of the materials are shown in Table 1.

Six sets of fiber orientations are considered. The fibers are oriented axially or circumferentially in one of the three layers and their direction changed in the other two layers. The fiber orientations in the outer, middle, and inner layers are shown, respectively, for six different sets:

Set 1	$0,\theta,-\theta$	Set 4	$\pi/2,\theta,-\theta$
Set 2	$-\theta,0,\theta$	Set 5	$-\theta,\pi/2,\theta$
Set 3	$\theta,-\theta,0$	Set 6	$\theta,-\theta,\pi/2$

where θ assumes values ranging from 0° to 90° with 10° intervals and is measured from the generatrix (see Fig. 1c). The fibers are axially oriented when θ is 0° and circumferentially oriented when it is 90°.

The numerical work was done with the aid of an IBM 7094 digital computer. A computer program was written to evaluate the stiffness parameters α, β, etc., and to solve Eqs. (26) and (30). The program options include a nonhomogeneous case where the coupling matrix $[D]$ is not equal to zero and an assumed homogeneous case where the matrix $[D]$ is set equal to zero.

From the numerical values, it is observed that for a given absolute value of angle θ, the following relations are valid for the stiffness parameters of different sets: 1) the parameters, β and γ, are nearly zero for all sets; 2) the values of the remaining parameters for sets 1 and 4 are the same as those for sets 3 and 6, respectively, except that κ, λ, and ψ have opposite signs; and 3) for sets 2 and 5 the stiffness parameters, ν, λ, and ψ, are zero. From these relations it is seen that for an assumed homogeneous case ($\nu = \xi = \kappa = \lambda = \psi = 0$) the buckling loads corresponding to sets 1 and 4 would be equal to those of sets 3 and 6, respectively.

The classical buckling loads for sets 1, 3, 4, and 6 for glass-epoxy and boron-epoxy composite cylindrical shells are plotted in Figs. 2 and 3. The classical buckling loads for sets 2 and 5 for boron-epoxy composite shells are given in Fig. 4.

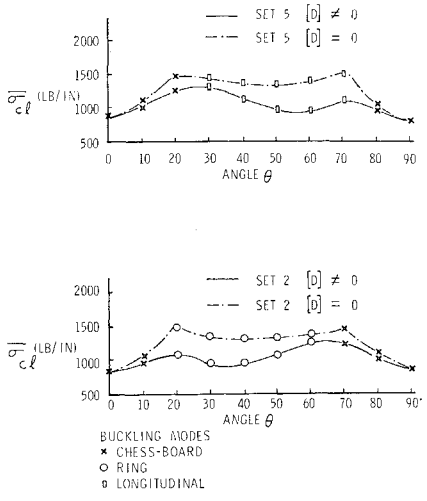

Fig. 4 Classical buckling loads for boron-epoxy composite shells.

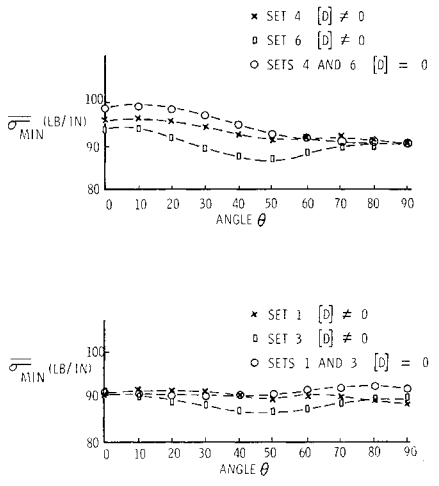

Fig. 6 Relative minimum postbuckling loads for N = 4 for glass-epoxy composite shells.

In these figures the value of $\bar{\sigma}_{cl}$ instead of the parameter, σ_{cl}, is plotted to facilitate comparison. The governing buckling mode is indicated at each point. It is evident from these plots that the assumption of homogeneity generally yields higher values of classical buckling loads (unconservative) and also that the governing buckling mode associated with the classical buckling load may be different. In particular for the boron-epoxy composite shell, the assumption of homogeneity gives 100% higher values for some fiber orientations. Among the fiber orientations investigated, those of orientation (0°, 70°, −70°) and (90°, 20°, −20°) yield the highest value of classical buckling load for both glass-epoxy and boron-epoxy composite shells. The values for these two materials are 575 lb/in. and 1385 lb/in., respectively. The ratios between the maximum and the minimum values of $\bar{\sigma}_{cl}$ are found to be 1.205 for glass-epoxy and 1.939 for boron-epoxy composite shells. The condition that the parameter, ω, must be a function of the integer value of the circumferential wave number, N, affects the classical buckling load in the chess board buckling mode only. It is observed that an imposition of this condition makes a very slight change in the numerical value of $\bar{\sigma}_{cl}$. N was found to be either 11 or 12 for glass-epoxy composite and its value varied from 10 to 13 for boron-epoxy composite shells.

The postbuckling curves, σ vs ε, for the glass-epoxy composite shell corresponding to fiber orientation (90°, 30°, −30°) and N = 4, 8, and 12 are shown in Fig. 5. Each curve in Fig. 5 indicates relative minimum postbuckling load. It was observed that the smallest value of this relative minimum is obtained when N = 4 for glass-epoxy and boron-epoxy composite shells. This is true for all fiber orientation and for nonhomogeneous as well as assumed homogeneous cases. For isotropic material the smallest value of the relative minimum postbuckling load ($\sigma_{\min}$) is 0.1549. This value which is in agreement with that given in Ref. 5 is also obtained when N = 4. It indicates that the circumferential wave number associated with the smallest value of the relative minimum postbuckling load primarily depends upon the radius-to-thickness ratio of the shell and appears to be independent of the material. The relative minimum postbuckling loads for sets 1, 3, 4, and 6 corresponding to N = 4 for nonhomogeneous ($[D] \neq 0$) and assumed homogeneous ($[D] = 0$) cases of glass-epoxy and boron-epoxy composite shells are plotted in Figs. 6 and 7. The values of end shortening, $\bar{\varepsilon}$, and wavelength ratio, $\bar{\mu}$, corresponding to these postbuckling loads are found to increase gradually for any set as the value of θ changes from 0° to 90°.

A close observation of Figs. 2–4, 6, and 7 would show that the classical buckling load for a given absolute value of θ for sets 1, 2, and 3 is the same as that for θ equal to (90° − θ) for sets 4, 5, and 6, respectively. But this is not true in the case of the relative minimum postbuckling loads. This happens because the principal axis of rigidity for the two cases is not the same.[6]

Although the minimum postbuckling loads may have little quantitative significance, they generally serve to indicate the degree of imperfection sensitivity of the shell. It is observed that the ratio $\bar{\sigma}_{\min}$ for N = 4 to $\bar{\sigma}_{cl}$ for a boron-epoxy composite shell is generally greater than that for a glass-epoxy shell for a given fiber orientation. This indicates that boron-epoxy composite shells are less imperfection sensitive than glass-epoxy composite shells (see Fig. 8).

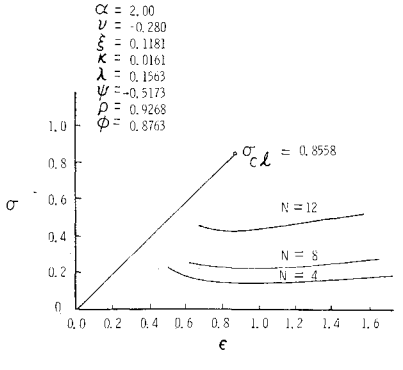

Fig. 5 Postbuckling curves for glass-epoxy composite cylindrical shell (90°,30°,−30°).

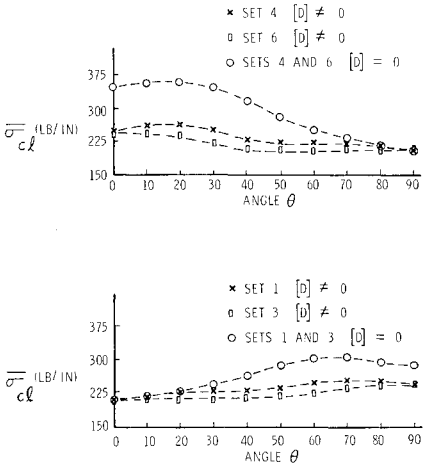

Fig. 7 Relative minimum postbuckling loads for N = 4 for boron-epoxy composite shells.

4. Initial Imperfections

The cylindrical shell passes through a maximum load state before it can snap through. This maximum load $\bar{\sigma}_{\max}$ which is of importance to the designer is influenced by the initial geometric imperfections in the shell.[10] $\bar{\sigma}_{\max}$ is equal to $\bar{\sigma}_{cl}$ if the shell is geometrically perfect. For the analysis of a geometrically imperfect shell, the initial imperfection is assumed to be of the form

$$\overline{W} = \overline{W}_1 \cos\frac{\pi x}{\bar{l}_x}\cos\frac{\pi y}{\bar{l}_y} + \overline{W}_2 \cos\frac{2\pi x}{\bar{l}_x} + \overline{W}_3 \cos\frac{2\pi x}{\bar{l}_x}\cos\frac{2\pi y}{\bar{l}_y} + \overline{W}_4 \cos\frac{4\pi x}{\bar{l}_y} \quad (32)$$

where $\overline{W}_1$ through $\overline{W}_4$ are the amplitudes of the imperfections and $\bar{l}_x$ and $\bar{l}_y$ are the half-wavelength in the axial and circumferential directions. The values of $\bar{l}_x$ and $\bar{l}_y$ are taken to be the same as those given by the classical chess board buckling mode.

The relative values of the imperfection amplitudes are set to

$$\overline{W}_1 = +4\overline{W}_2 = -4\overline{W}_3 = 16\overline{W}_4$$

which are the same as those given by Yoshimura buckling pattern.[10] The imperfection ratio $\overline{W}^*$ is defined here as the ratio of $W_1 + W_2 + W_3 + W_4$ to the thickness of the shell. The analytical formulation for investigating the influence of initial imperfections is not given in this paper for want of space.

In Fig. 8, the ratios $\bar{\sigma}_{\max}$ to $\bar{\sigma}_{cl}$ for the imperfection ratio $\overline{W}^* = 0.04$ are plotted for glass-epoxy and boron-epoxy composite shells for the fiber orientations of set 6. For boron-epoxy composites for θ equal to 40°, the value is not plotted since the load-shortening curve does not indicate snap-through, but it increases monotonically. It is noticed that as the value of $\overline{W}^*$ is increased, more fiber orientations fall under this category for boron-epoxy composite than for glass-epoxy composite shells. In order to find snap-buckling load for larger values of $\overline{W}^*$, it seems it is necessary to use a more complete expression for the radial displacement function W than the one used in Eq. (17). It is evident from Figs. 2, 3, and 8 that an increase in σ_{cl} due to change in fiber orientation is accompanied by an increase in imperfection sensitivity of the cylindrical shell. The ratios $\bar{\sigma}_{\min}$ for $N = 4$ to $\bar{\sigma}_{cl}$ are also plotted in the same figure. From the limited data collected, it is observed that initial imperfections have less influence on the buckling behavior of the boron-epoxy composite than on the glass-epoxy composite shells, the composite cylindrical shells seem to be less imperfection sensitive than isotropic shells.

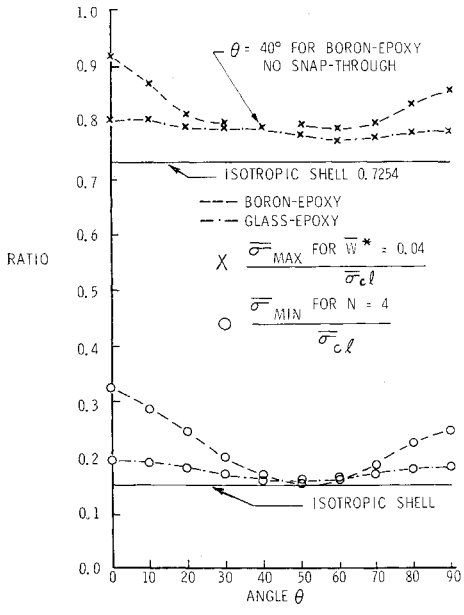

Fig. 8 The ratios [$\bar{\sigma}_{\min}$ for $N = 4/\bar{\sigma}_{cl}$ [and [$\bar{\sigma}_{\max}$ for $\overline{W}^* = 0.04/\bar{\sigma}_{cl}$] for glass-epoxy and boron-epoxy composite shells for set 6.

Appendix A

$$\bar{F} = F_1\cos\frac{\pi x}{l_x}\cos\frac{\pi y}{l_y} + F_2\sin\frac{\pi x}{l_x}\sin\frac{\pi y}{l_y} + F_3\cos\frac{2\pi x}{l_x} + F_4\cos\frac{2\pi y}{l_y} + F_5\cos\frac{2\pi x}{l_x}\cos\frac{2\pi y}{l_y} + F_6\sin\frac{2\pi x}{l_x}\sin\frac{2\pi y}{l_y} + F_7\cos\frac{3\pi x}{l_x}\cos\frac{\pi y}{l_y} + F_8\sin\frac{3\pi x}{l_x}\sin\frac{\pi y}{l_y} + F_9\cos\frac{\pi x}{l_x}\cos\frac{3\pi y}{l_y} + F_{10}\sin\frac{\pi x}{l_x}\sin\frac{3\pi y}{l_y} + F_{11}\cos\frac{4\pi x}{l_x} + F_{12}\cos\frac{4\pi y}{l_y} + F_{13}\cos\frac{4\pi x}{l_x}\cos\frac{2\pi y}{l_y} + F_{14}\sin\frac{4\pi x}{l_x}\sin\frac{2\pi y}{l_y} + F_{15}\cos\frac{5\pi x}{l_x}\cos\frac{\pi y}{l_y} + F_{16}\sin\frac{5\pi x}{l_x}\sin\frac{\pi y}{l_y} + F_{17}\cos\frac{6\pi x}{l_x}\cos\frac{2\pi y}{l_y} + F_{18}\sin\frac{6\pi x}{l_x}\sin\frac{2\pi y}{l_y}$$

where

$$F_1 = \left[-\left\{W_1\left(G_1 - \frac{l_y^2}{R\pi^2}\right) + 2W_1W_2\right\} \times G_2 - W_1G_3G_4\right] \Big/ (G_2^2 - G_4^2)$$

$$F_2 = \left[W_1G_3G_2 + \left\{W_1\left(G_1 - \frac{l_y^2}{R\pi^2}\right) + 2W_1W_2\right\} \times G_4\right] \Big/ (G_2^2 - G_4^2)$$

$$F_3 = W_2\left\{-\frac{d_{12}}{a_{22}} + \frac{l_y^2}{4\bar{\mu}^2a_{22}R\pi^2}\right\} - \frac{1}{32}\frac{W_1^2}{\bar{\mu}^2a_{22}}$$

$$F_4 = -W_1^2\left\{\frac{1}{32\bar{\eta}^2a_{11}}\right\} - W_2W_3\left\{\frac{1}{2\bar{\eta}^2a_{11}}\right\}$$

$$F_5 = \left[-\left\{W_3\left(G_1 - \frac{l_y^2}{4R\pi^2}\right) + 2W_3W_4\right\} \times G_2 - W_3G_3G_4\right] \Big/ (G_2^2 - G_4^2)$$

$$F_6 = \left[W_3G_3G_2 + \left\{W_3\left(G_1 - \frac{l_y^2}{4R\pi^2}\right) + 2W_2W_4\right\} \times G_4\right] \Big/ (G_2^2 - G_4^2)$$

$$F_7 = -[4W_1W_3 + 2W_1W_2 + 8W_1W_4]G_5/(G_5^2 - G_6^2)$$

$$F_8 = [4W_1W_3 + 2W_1W_2 + 8W_1W_4]G_6/(G_5^2 - G_6^2)$$

$$F_9 = -4W_1W_3G_7/(G_7^2 - G_8^2)$$

$$F_{10} = 4W_1W_3G_8/(G_7^2 - G_8^2)$$

$$F_{11} = W_4\left\{-\frac{d_{12}}{a_{22}} + \frac{l_y^2}{16\bar{\mu}^2a_{22}\pi^2R}\right\} - \frac{1}{32\bar{\mu}^2a_{22}}W_3^2$$

$$F_{12} = -W_3^2/32\bar{\eta}^2a_{11}$$

$$F_{13} = -W_2W_3G_9/(G_9^2 - G_{10}^2)$$

$$F_{14} = W_2W_3G_{10}/(G_9^2 - G_{10}^2)$$

$$F_{15} = -8W_1W_4G_{11}/(G_{11}^2 - G_{12}^2)$$

$$F_{16} = 8W_1W_4G_{12}/(G_{11}^2 - G_{12}^2)$$

$$F_{17} = -2W_3W_4G_{13}/(G_{13}^2 - G_{14}^2)$$
$$F_{18} = 2W_3W_4G_{14}/(G_{13}^2 - G_{14}^2)$$
$$\bar{\mu} = l_y/l_x \qquad \bar{\eta} = l_x/l_y$$
$$G_1 = d_{12}\bar{\mu}^2 + d_{21}\bar{\eta}^2 + (d_{11} + d_{22} - 2d_{66})$$
$$G_2 = a_{22}\bar{\mu}^2 + a_{11}\bar{\eta}^2 + (2a_{12} + a_{66})$$
$$G_3 = (2d_{62} - d_{16})\bar{\mu} + (2d_{61} - d_{26})\bar{\eta}$$
$$G_4 = 2\bar{\mu}a_{26} + 2\bar{\eta}a_{16}$$
$$G_5 = 81a_{22}\bar{\mu}^2 + a_{11}\bar{\eta}^2 + 9(2a_{12} + a_{66})$$
$$G_6 = 54\bar{\mu}a_{26} + 6\bar{\eta}a_{16}$$
$$G_7 = a_{22}\bar{\mu}^2 + 81a_{11}\bar{\eta}^2 + 9(2a_{12} + a_{66})$$
$$G_8 = 6\bar{\mu}a_{26} + 54\bar{\eta}a_{16}$$
$$G_9 = 32a_{22}\bar{\mu}^2 + 2a_{11}\bar{\eta}^2 + 8(2a_{12} + a_{66})$$
$$G_{10} = 32\bar{\mu}a_{26} + 8\bar{\eta}a_{16}$$
$$G_{11} = 625a_{22}\bar{\mu}^2 + a_{11}\bar{\eta}^2 + 25(2a_{12} + a_{66})$$
$$G_{12} = 250\bar{\mu}a_{26} + 10\bar{\eta}a_{16}$$
$$G_{13} = 81a_{22}\bar{\mu}^2 + a_{11}\bar{\eta}^2 + 9(2a_{12} + a_{66})$$
$$G_{14} = 54a_{26}\bar{\mu} + 6a_{16}\bar{\eta}$$

Appendix B

$$T_1 = \mu^4 + \alpha\mu^2 + 1 \qquad T_2 = 2\mu(\mu^2\beta + \gamma)$$
$$T_3 = \kappa\mu^4 + \psi\mu^2 + \lambda - \mu^2\omega \qquad T_4 = \mu(\nu\mu^2 + \xi)$$
$$T_5 = 81\mu^4 + 9\alpha\mu^2 + 1 \qquad T_6 = 6\mu(9\mu^2\beta + \gamma)$$
$$T_7 = \mu^4 + 9\alpha\mu^2 + 81 \qquad T_8 = 6\mu(\mu^2\beta + 9\gamma)$$
$$T_9 = 625\mu^4 + 25\alpha\mu^2 + 1 \qquad T_{10} = 10\mu(25\mu^2\beta + \gamma)$$
$$T_{11} = 16\mu^4 + 4\alpha\mu^2 + 1 \qquad T_{12} = 4\mu(4\mu^2\beta + \gamma)$$
$$T_{13} = \kappa\mu^4 + \psi\mu^2 + \lambda - \omega\mu^2/4$$

Appendix C

$$R_1 = 1/(H_1^2 - 4aH_2^2)$$
$$R_2 = \tfrac{1}{2}[H_1H_3^2/a + H_1H_4^2 + 4H_2H_3H_4]$$
$$R_3 = H_1a/2$$
$$R_4 = -H_1H_3 - 2aH_2H_4$$
$$R_5 = H_5/2a$$
$$R_6 = R_1^2[4H_2^2 + 8aH_2\beta - 2H_1H_6]$$
$$R_7 = \frac{1}{2}\left[-\frac{1}{a^2}H_1H_3^2 + \frac{1}{a}\{H_6H_3^2 + 2H_1H_3H_7\} + H_6H_4^2 + 2H_1H_4\nu + 4H_3H_4\beta + 4H_2H_3\nu + 4H_2H_4H_7\right]$$
$$R_8 = H_1/a + H_6a/2$$
$$R_9 = -[H_6H_3 + H_7H_1 + 2H_2H_4 + 2a\beta H_4 + 2a\nu H_2]$$
$$R_{10} = -H_5/2a^2 + (1/2a)(2\rho\phi^{1/2} + 2\phi a)$$
$$R_{11} = R_1R_7 + R_2R_6 + R_{10} \qquad R_{12} = R_1R_8 + R_3R_6$$
$$R_{13} = R_1R_9 + R_4R_6$$
$$H_1 = a^2 + a\alpha + 1 \qquad H_2 = a\beta + \gamma$$
$$H_3 = \kappa a^2 + \psi a + \lambda \qquad H_4 = \nu a + \xi$$
$$H_5 = 1 + 2a\rho\phi^{1/2} + \phi a^2 \qquad H_6 = 2a + \alpha$$
$$H = 2\kappa a + \psi \qquad a = \mu^2$$

References

[1] Tasi, J., Feldman, A., and Stang, D. A., "The Buckling Strength of Filament-Wound Cylinders Under Axial Compression," CR-266, 1965, NASA.

[2] Tasi, J., "Effect of Heterogeneity on the Stability of Composite Cylindrical Shells under Axial Compression," *AIAA Journal*, Vol. 4, No. 6, June 1966, pp. 1058–1062.

[3] von Kármán, T. and Tsien, H. S., "The Buckling of Thin Cylindrical Shells under Axial Compression," *Journal of the Aeronautical Sciences*, Vol. 8, No. 8, June 1941, pp. 303–312.

[4] Kempner, J., "Postbuckling Behavior of Axially Compressed Circular Cylindrical Shells," *Journal of the Aeronautical Sciences*, Vol. 21, No. 5, May 1954, pp. 329–335.

[5] Almroth, B. O., "Postbuckling Behavior of Axially Compressed Circular Cylinders," *AIAA Journal*, Vol. 1, No. 3, March 1963, pp. 630–633.

[6] Thielemann, W. F., "New Developments in the Nonlinear Theories of the Buckling of Thin Cylindrical Shells," *Proceedings of the Durand Centennial Conference*, Pergamon Press, New York, 1960, p. 76.

[7] Thielemann, W. F., "On the Postbuckling Behavior of Thin Cylindrical Shells," TN D-1510, 1962, NASA, p. 203.

[8] Almroth, B. O., "Postbuckling Behavior of Orthotropic Cylinders under Axial Compression," *AIAA Journal*, Vol. 2, No. 10, Oct. 1964, pp. 1795–1799.

[9] Hoff, N. J., Madsen, W. A., and Mayers, J., "Postbuckling Equilibrium of Axially Compressed Circular Cylindrical Shells," *AIAA Journal*, Vol. 4, No. 1, Jan. 1966, pp. 126–133.

[10] Madsen, W. A. and Hoff, N. J., "The Snap-Through and Postbuckling Equilibrium Behavior of Circular Shells Under Axial Load," SUDAER 277, 1965, Dept. Aeronautics and Astronautics, Stanford Univ.

[11] Hoff, N. J., "The Perplexing Behavior of Thin Cylindrical Shells in Axial Compression," *Proceedings of the VIIIth Israel Annual Conference on Aviation and Astronautics*, Feb. 1966.

[12] Tsai, S. W., "Mechanics of Composite Materials," Rept. TR-66-149, Pt. 2, 1966, Air Force Materials Lab.